Atom–atom interactions around the band edge of a photonic crystal waveguide

Jonathan D. Hood[a,b], Akihisa Goban[a,b,1], Ana Asenjo-Garcia[a,b], Mingwu Lu[a,b], Su-Peng Yu[a,b], Darrick E. Chang[c], and H. J. Kimble[a,b,2]

[a]Norman Bridge Laboratory of Physics MC12-33, California Institute of Technology, Pasadena, CA 91125; [b]Institute for Quantum Information and Matter, California Institute of Technology, Pasadena, CA 91125; and [c]Institut de Ciencies Fotoniques, The Barcelona Institute of Science and Technology, 08860 Barcelona, Spain

Contributed by H. Jeffrey Kimble, June 17, 2016 (sent for review March 7, 2016; reviewed by Eugene Polzik and Dan Stamper-Kurn)

Tailoring the interactions between quantum emitters and single photons constitutes one of the cornerstones of quantum optics. Coupling a quantum emitter to the band edge of a photonic crystal waveguide (PCW) provides a unique platform for tuning these interactions. In particular, the cross-over from propagating fields $E(x) \propto e^{\pm ik_x x}$ outside the bandgap to localized fields $E(x) \propto e^{-\kappa_x |x|}$ within the bandgap should be accompanied by a transition from largely dissipative atom–atom interactions to a regime where dispersive atom–atom interactions are dominant. Here, we experimentally observe this transition by shifting the band edge frequency of the PCW relative to the D_1 line of atomic cesium for $\bar{N} = 3.0 \pm 0.5$ atoms trapped along the PCW. Our results are the initial demonstration of this paradigm for coherent atom–atom interactions with low dissipation into the guided mode.

quantum optics | nanophotonics | atomic physics

Recent years have witnessed a spark of interest in combining atoms and other quantum emitters with photonic nanostructures (1). Many efforts have focused on enhancing emission into preferred electromagnetic modes relative to vacuum emission, thereby establishing efficient quantum matter–light interfaces and enabling diverse protocols in quantum information processing (2). Photonic structures developed for this purpose include high-quality cavities (3–7), dielectric fibers (8–13), metallic waveguides (14–16), and superconducting circuits (17–19). Photonic crystal waveguides (PCWs) are of particular interest, because the periodicity of the dielectric structure drastically modifies the field propagation, yielding a set of Bloch bands for the guided modes (GMs) (20). For example, recent experiments have shown superradiant atomic emission because of a reduction in group velocity for an atomic frequency near a band edge of a PCW (21).

A quite different paradigm for atom–light interactions in photonic crystals was proposed in the works in refs. 22–25 but has yet to be experimentally explored. In particular, when an atomic transition frequency is situated within a bandgap of a PCW, an atom can no longer emit propagating waves into GMs of the structure. However, an evanescent wave surrounding the atoms can still form, resulting in the formation of atom–photon-bound states (26, 27). This phenomenon has attracted new interest recently as a means to realize dispersive interactions between atoms without dissipative decay into GMs. The spatial range of atom–atom interactions is tunable for 1D and 2D PCWs and set by the size of the photonic component of the bound state (28, 29). Many-body physics with large spin exchange energies and low dissipation can thereby be realized in a generalization of cavity quantum electrodynamics (CQED) arrays (30, 31). Fueled by such perspectives, there have been recent experimental observations with atoms (21, 32, 33) and quantum dots (34, 35) interacting through the GMs of PCWs, albeit in frequency regions outside the bandgap, where GMs are propagating fields.

In this manuscript, we report the observation of collective dispersive shifts of the atomic resonance around the band edge of a photonic crystal. Thermal tuning allows us to control the offset of the band edge frequency (ν_{BE}) of the PCW relative to the frequency ν_{D1} of the D_1 line of cesium (Cs). In both the dispersive domain [i.e., ν_{D1} outside the bandgap with electric field $E(x) \propto e^{\pm ik_x x}$] and reactive regime [i.e., ν_{D1} inside the bandgap with $E(x) \propto e^{-\kappa_x |x|}$], we record transmission spectra for atoms trapped along the PCW, as illustrated in Fig. 1*A*.

To connect the features of the measured transmission spectra to underlying atom–atom radiative interactions, we have developed a formalism based on the electromagnetic Green's function. The model allows us to infer the peak single-atom frequency shift of the atomic resonance $J_{1D}(\Delta_{BE})$ and GM decay rate $\Gamma_{1D}(\Delta_{BE})$ as functions of detuning $\Delta_{BE} = \nu_{D1} - \nu_{BE}$ between the atomic ν_{D1} and band edge ν_{BE} frequencies. From the observation of superradiant emission outside the bandgap, we infer the average number of trapped atoms to be $\bar{N} = 3.0 \pm 0.5$, as described in ref. 21 and *SI Text*. (*SI Text* has thorough descriptions of the design and characterization of the PCW, how to obtain the attenuation coefficient and the band edge position of the PCW, how to generate the atomic spectra fits, and the measurements of atomic decay.) For frequencies inside the bandgap ($\Delta_{BE} = 50$ GHz), the ratio of dissipative to coherent rates is $\mathcal{R} = \Gamma_{1D}/J_{1D} = 0.05 \pm 0.17$ because of the exponential localization of the atomic radiation in the bandgap. For comparison, the prediction for our system from CQED models alone is $\mathcal{R}_{CQED} = 0.30 \pm 0.04$. Other than yielding a more favorable ratio between coherent and dissipative GM rates, PCWs offer significant advantages compared with conventional cavities as

Significance

In recent years, there has been considerable effort to bring ultracold atoms into the realm of nanophotonics. Nanoscopic dielectric devices offer unprecedented opportunities to engineer novel capabilities for the control of atom–photon interactions. In particular, photonic crystals are periodic dielectric structures that display a photonic bandgap where light cannot propagate and provide a new setting for coherent photon-mediated interactions between atoms with tunable range. Here, we report the initial observation of cooperative atom–atom interactions around the band edge of a photonic crystal waveguide. Our experiment opens the door to fascinating scenarios, such as exploring many-body physics with large spin exchange energies and low dissipation.

Author contributions: J.D.H., A.G., S.-P.Y., and H.J.K. designed research; J.D.H., A.G., A.A.-G., M.L., S.-P.Y., D.E.C., and H.J.K. performed research; J.D.H., A.G., A.A.-G., S.-P.Y., and D.E.C. contributed new reagents/analytic tools; J.D.H., A.G., A.A.-G., M.L., and S.-P.Y. analyzed data; and J.D.H., A.A.-G., and H.J.K. wrote the paper.

Reviewers: E.P., Copenhagen University; and D.S.-K., University of California, Berkeley.

The authors declare no conflict of interest.

Freely available online through the PNAS open access option.

[1]Present address: JILA, University of Colorado, Boulder, CO 80309.

[2]To whom correspondence should be addressed. Email: hjkimble@caltech.edu.

This article contains supporting information online at www.pnas.org/lookup/suppl/doi:10.1073/pnas.1603788113/-/DCSupplemental.

platforms for atom–light interfaces. First, the range of interaction in a PCW is tunable, ranging from effectively infinite to nearest neighbor (28, 29, 36), in contrast to the fixed infinite range of a cavity. Second, because of the multimode nature of PCWs, one can use different GMs as different interaction channels to which the atoms simultaneously couple.

Alligator PCW

Fig. 1*A* provides an overview of our experiment with atoms trapped near and strongly interacting with the transverse-electric (TE) mode of an alligator PCW. The suspended silicon nitride (SiN) structure consists of $N_{\text{cells}} = 150$ nominally identical unit cells of lattice constant $a = 370$ nm and is terminated by 30 tapering cells on each side, as shown in the SEM images in Fig. 1*B*. The tapers mode-match the fields of the PCW to the fields of uncorrugated nanobeams for efficient input and output coupling. Design, fabrication, and characterization details are described in refs. 21, 32, and 33. Fig. 1*C* shows the nominal cell dispersion relations for the TE (polarized mainly along y) and transverse-magnetic (TM) modes (polarized mainly along z). After release of the SiN structure from the silicon (Si) substrate, a low-power CF_4 etch is used to align the lower/"dielectric" TE band edge (ν_{BE}) to the Cs D_1 transition (ν_{D1}). The TM mode has band edges far detuned from the both the Cs D_1 and D_2 lines. In our experiment, the TE mode is used to probe the atoms, whereas the TM mode with approximately linear dispersion serves to calibrate the density and trap properties.

To better understand atomic interactions with the PCW, it is helpful to visualize the spatial profile of the fields generated absent atoms, when light is input from one end. Fig. 2*A* shows the measured intensity along the length of the PCW as a function of probe detuning $\delta_{\text{BE}} = \nu_p - \nu_{\text{BE}}$ around the band edge, where ν_p is the probe frequency. The intensity was measured by imaging weak scatterers along the length of the alligator PCW that, after calibration, serve as local probes of the intensity (*SI Text*). Fig. 2*B* shows the corresponding finite difference time domain (FDTD) simulated intensity (37). In both images, resonances appear at $\nu_p = \nu_{1,2,3}$ because of the weak cavity formed by the reflections of the tapers. The spatial modulation of the intensity at the resonances caused by the cavity effect is approximated by $|E(x)|^2 \approx \cos^2(\delta k_x\, x)$, where $\delta k_x = \pi/a - k_x$ is the effective wavevector near the band edge. The nth resonance at frequency ν_n is such that $\delta k_x = n\pi/L$, where L is the effective length of the PCW (including field penetration into the tapers). Fig. 2*C* shows a plot of $|E(x)|^2$ for a probe input at frequency $\nu_p = \nu_1$ at the first resonance. Inside the bandgap ($\Delta_{\text{BE}} > 0$), the field is evanescent, and $\delta k_x = i\kappa_x$. Fig. 2*D* plots $|E(x)|^2$ for probe frequency $\nu_p = \nu_{\text{BG}}$ inside the bandgap and shows the exponential decay of the intensity. Using a model for the field in a finite photonic crystal (*SI Text*), we fit the measured intensity for each frequency in Fig. 2 *A* and *B* and extract δk_x and κ_x, thereby obtaining the dispersion relations shown in Fig. 2*E*. Importantly, we determine the band edge frequency for the actual device to be $\nu_{\text{BE}} - \nu_1 = 133 \pm 9$ GHz relative to the readily measured first resonance at ν_1, which is in good agreement with the FDTD-simulated result of 135 GHz.

Both ν_1 and ν_{BG} are relevant to our measurements of transmission spectra with trapped atoms. The presence of a "cavity" mode at ν_1 implies that the emission of an atom with transition frequency $\nu_{\text{D1}} = \nu_1$ will generate a field inside the PCW with an analogous spatial profile to that of the cavity mode, as shown in Fig. 2*C*. By contrast, atomic emission in the regime with $\nu_{\text{D1}} = \nu_{\text{BG}}$ within the bandgap will excite an exponentially localized mode centered around the atomic position x_{A}, as illustrated in Fig. 2*F*.

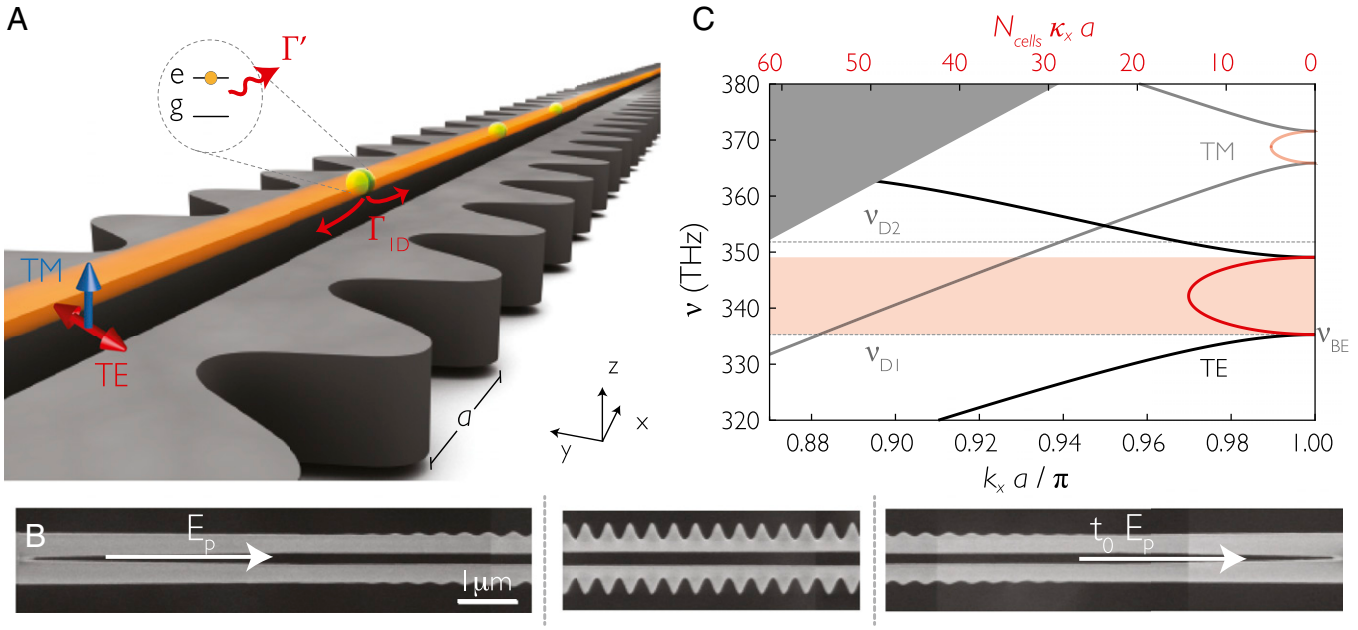

Fig. 1. Description of the alligator PCW. (*A*) Atoms are trapped above the PCW in an optical dipole trap formed by the reflection of a near-normal incidence external beam (21). The orange cylinder represents the confinement of the atoms, which is $\Delta x_{\text{A}} \simeq \pm 6$ μm along the axis of the device and $\Delta y_{\text{A}} \simeq \Delta z_{\text{A}} \simeq \pm 30$ nm in the transverse directions (*SI Text*). The three green spheres represent trapped atoms that interact radiatively through the fundamental TE GM, polarized mainly along y. The decay rate for a single atom into the PCW is $\Gamma_{1\text{D}}$ (red arrows), and the decay rate into all other modes is Γ' (wavy red arrow). (*B*) SEM images of portions of the tapering and PCW sections. The suspended SiN device (gray) consists of 150 cells and 30 tapering cells on each side. The lattice constant is $a = 370$ nm, and thickness is 185 nm. (*C*) Calculated band structure of the fundamental TE (solid) and TM (translucent) modes using an eigenmode solver (38) and the measured SEM dimensions, which are modified within their uncertainty to match the measured bands. The black curves represent the Bloch wavevector k_x (lower axis). The red curves show the attenuation coefficient κ_x of the field for frequencies in the bandgap (upper axis) and are calculated by means of an analytical model (*SI Text*). The dotted lines mark the frequencies of the Cs D_1 ($\nu_{\text{D1}} = 335.1$ THz) and D_2 ($\nu_{\text{D2}} = 351.7$ THz) transitions. The dielectric band edge is indicated as ν_{BE}. The pink shaded area represents the TE bandgap. The gray shaded area represents the light cone.

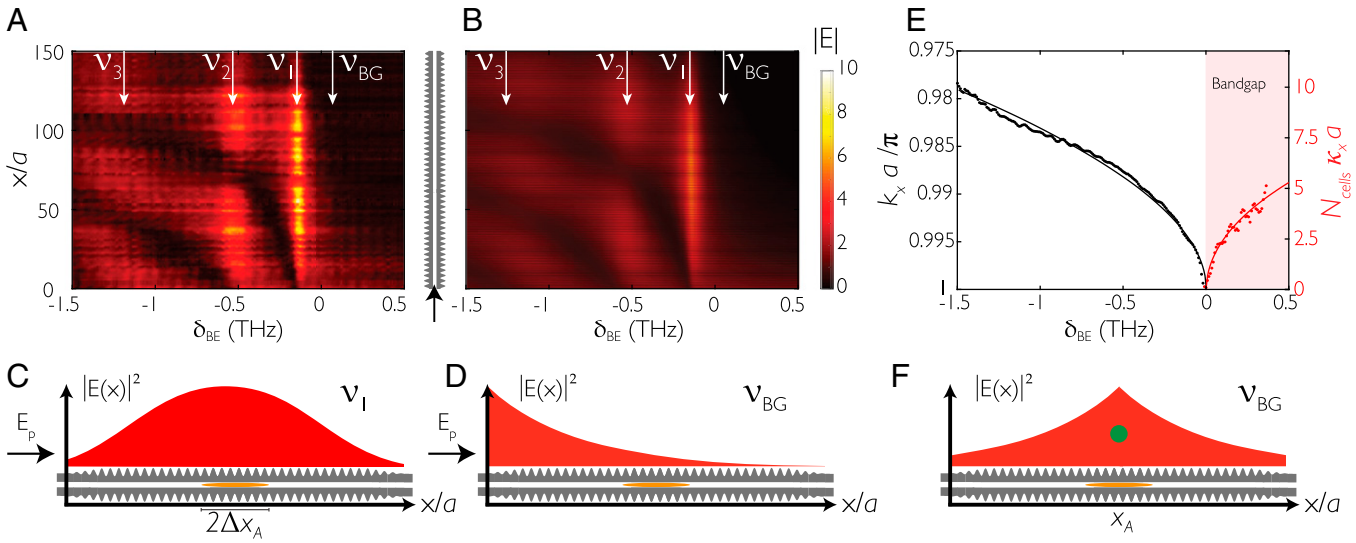

Fig. 2. Characterization of the alligator PCW. (*A*) Measured and (*B*) calculated electric field magnitudes along the PCW as functions of position x along the PCW and probe detuning $\delta_{BE} = \nu_p - \nu_{BE}$ relative to ν_{BE} for the dielectric band edge. (*C* and *D*) GM intensity $|E(x)|^2$ along PCW at two different frequencies: (*C*) ν_1 for the first cavity resonance showing a resonant "supermode" and (*D*) ν_{BG} inside the bandgap displaying exponential decay ($N_{cells}\kappa_x a = 2.0$ at ν_{BG}). For clarity, the number of cells of the nominal and tapering sections is decreased by a factor of five, and the Bloch periodicity ($a = 370$ nm), although present, is not shown in the intensity. The orange ovals represent the confinement of the atoms in the optical trap above the PCW, which is $\Delta x_A \simeq \pm 6$ μm along the x axis of the device and $\Delta y_A \simeq \pm 30$ nm, with a PCW gap width of 220 nm. (*E*) Dispersion relation for the projected wavevector k_x and attenuation constant κ_x vs. probe detuning δ_{BE} deduced for the PCW obtained by fitting the data in *A* to a model of the device (*SI Text*). The shaded pink area represents frequencies inside the bandgap. (*F*) Plot of the exponentially localized emission $e^{-2\kappa_x|x-x_A|}$ from an atom (green sphere) at position x_A with transition frequency $\nu_{D1} = \nu_{BG}$ inside the bandgap.

Experiment

Cs atoms are trapped above the surface of the alligator PCW, as shown in Fig. 1*A*, using a similar experimental setup to that reported in ref. 21. As described in more detail in ref. 21, the decay rate Γ_{1D} into the GM is exponentially sensitive to the trap position above the surface of the alligator PCW. Our calculations and measurements of Γ_{1D} agree with COMSOL simulations (38) of the trap position, and thus, we are able to determine that the Cs atoms are trapped 145 ± 15 nm above the surface of the alligator PCW. Atoms are cooled and trapped in a magneto-optical trap (MOT) around the PCW and then loaded into a dipole trap formed by the reflection from the device of a frequency red-detuned side illumination (SI) beam. The SI beam has a waist of 50 μm, and the polarization is aligned along the x axis for maximum reflection from the PCW. We measure a $1/e$ trap lifetime of ~ 30 ms, and we estimate an atom temperature of ~ 30 μK from time of flight measurements. From the trap simulations (details are in *SI Text*), we infer that the atoms are confined to a region 145 nm above the surface with dimensions $\Delta x_A \simeq \pm 6$ μm and $\Delta y_A \simeq \Delta z_A \simeq \pm 30$ nm. The simulations predict that more energetic atoms escape the trap and collide into the structure, because the weakest direction of the trap is along the diagonals of the y–z plane due to Casimir–Polder forces.

To estimate the average number of trapped atoms, we measure the superradiant atomic decay rate when the atom frequency ν_{D1} is tuned to the first resonance ν_1 of the PCW (Fig. 2*C*) (21). Because of the strong dissipative interactions between the atoms and with $J_{1D} \approx 0$, the collective decay rate is enhanced compared with the single-atom decay rate, and we infer an average atom number of $\bar{N} = 3.0 \pm 0.5$ (*SI Text*). In the low-density limit $\bar{N} \ll 1$, the measured decay rate corresponds to that of a single atom. We then measure a GM decay rate $\Gamma_{1D} = (1.5 \pm 0.2)\,\Gamma_0$, which is in good agreement with the FDTD simulations at the calculated trap location (*SI Text*).

After the atoms are loaded into the trap, we send a weak 5-ms probe beam E_p with frequency ν_p in either the TE or TM GM through the PCW and record the transmitted intensity $\left|t(\nu_p)\, E_p(\nu_p)\right|^2$. The probe beam scans near the Cs $6S_{1/2}, F = 3 \rightarrow 6P_{1/2}, F' = 4$ transition. Each experimental cycle runs at a fixed detuning $\Delta_A = \nu_p - \nu_{D1}$

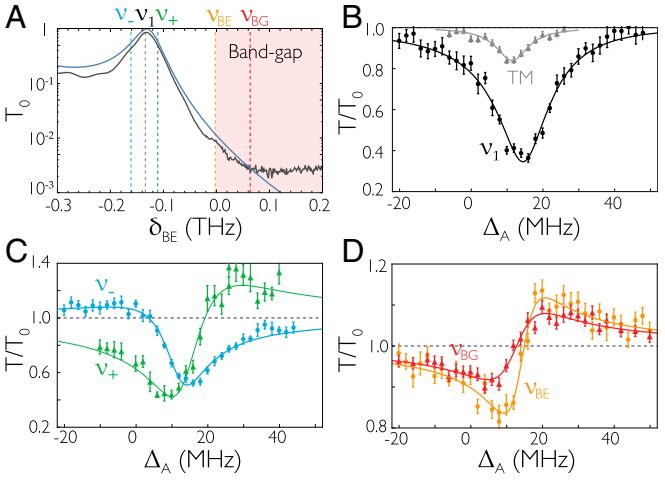

Fig. 3. Transmission spectra of the PCW (*A*) without and (*B–D*) with trapped atoms. (*A*) Measured (black) and FDTD-simulated (blue) transmission spectra of the PCW without atoms as a function of the probe detuning from the band edge frequency, $\delta_{BE} = \nu_p - \nu_{BE}$. There is a minimum extinction of 25 dB for the transmitted signal because of fabrication imperfections. (*B–D*) Transmission spectrum for $\bar{N} = 3.0 \pm 0.5$ trapped atoms vs. probe detuning $\Delta_A = \nu_p - \nu_{D1}$ at several frequencies around the band edge. The solid lines are fits using the transmission model in Eq. **4** averaged over atom positions and different atom numbers. In *B*, the Cs D_1 line is aligned to the first cavity resonance ν_1, resulting in symmetric spectra for both the TE (black; ●) and TM (gray; ▲) modes. The TE spectra in *C* are for frequencies on the negative side (ν_-; ●) and positive side (ν_+; ▲) of the ν_1 resonance. The TE spectra in *D* are taken at the band edge (ν_{BE}; ●) and 60 GHz (ν_{BG}; ▲) into the bandgap. The asymmetry of the line shapes in *C* and *D* implies a large ratio of coherent to dissipative interactions.

relative to the free space atomic transition frequency ν_{D1}. We observe little change of signal during the 5-ms probing time, suggesting that the atom number is approximately constant over this interval. The band edge of the PCW is tuned thermally by shining an external laser onto a corner of the chip, where its light is absorbed by the Si substrate. Hence, the Cs D_1 line can be aligned to be either outside or inside the bandgap with an uncertainty $\delta\nu \simeq 5$ GHz. The transmission for each data point is normalized by the transmission with no atoms ($|t_0 E_p|^2$), resulting in a measurement of $T/T_0 \equiv |t/t_0|^2$. The logarithm of the measured and simulated transmission spectra with no atoms $T_0 = |t_0(\nu_p)|^2$ is shown in Fig. 3*A*.

Examples of transmission spectra with atoms are shown in Fig. 3 *B–D*. Note that the spectra are shifted 12.5 MHz because of both the alternating current (AC) Stark shift of the dipole trap and the modified Lamb shift induced by the non-GMs of the PCW. Notably, the transmission spectra at the first cavity resonance ν_1 exhibit a characteristic Lorentzian "dip," and they become more asymmetric as the frequency moves into the bandgap.

Transmission Model

We have developed a model to extract quantitative values for collective decay rates and frequency shifts from these atomic transmission spectra (39). Although the formalism of waveguide (40) and CQED (41) is well-suited for describing atoms coupled to uniform waveguides and cavities, it is not general enough to capture the rich physics of atomic interactions in the vicinity of a PCW. Instead, we describe our system by using a spin model in terms of the classical electromagnetic Green's function, in which the atoms (or "pseudospins" for ground and excited states) interact through the emission and reabsorption of guided photons (42–44).

The electromagnetic Green's tensor $\mathbf{G}(\mathbf{r}, \mathbf{r}_i, \omega)$ is related to the electric field $\mathbf{E}(\mathbf{r}, \omega)$ emitted by a dipole $\mathbf{p}_i$ oscillating at frequency ω at position $\mathbf{r}_i$ by $\mathbf{E}(\mathbf{r}, \omega) = \mu_0 \omega^2 \mathbf{G}(\mathbf{r}, \mathbf{r}_i, \omega) \cdot \mathbf{p}_i$ (43, 45). The dipole moment operator for atom i is decomposed into $\hat{\mathbf{p}}_i = \mathbf{d}_i \hat{\sigma}^i_{ge} + \mathbf{d}_i^* \hat{\sigma}^i_{eg}$, where $\mathbf{d}_i$ is the dipole matrix element and $\hat{\sigma}^i_{ge} = |g\rangle\langle e|$ is the atomic coherence operator between the ground and excited states. The spin model describes a system of N atoms coupled to and driven by a GM of the PCW. In the low-saturation and steady-state regime, expectation values for the atomic coherences ($\sigma^i_{ge} = \langle \hat{\sigma}^i_{ge} \rangle$) are described by a linear system of equations (39) (*SI Text*):

$$\left(\tilde{\Delta}_A + \mathrm{i}\frac{\Gamma'}{2}\right)\sigma^i_{ge} + \sum_{j=1}^{N} g_{ij}\,\sigma^j_{ge} = -\Omega_i, \qquad [1]$$

where $\tilde{\Delta}_A = 2\pi\Delta_A = 2\pi(\nu_p - \nu_{D1})$ is the detuning between the probe and the atomic angular frequencies, Ω_i is the classical drive (Rabi frequency) for the ith atom due to the GM input field, and $g_{ij} = J^{ij}_{1D} + \mathrm{i}\Gamma^{ij}_{1D}/2$, where $J^{ij}_{1D} = \mu_0 \omega_p^2/\hbar\ \mathbf{d}_i^* \cdot \mathrm{Re}\ \mathbf{G}(\mathbf{r}_i, \mathbf{r}_j, \omega_p) \cdot \mathbf{d}_j$ and $\Gamma^{ij}_{1D} = 2\mu_0\ \omega_p^2/\hbar\ \mathbf{d}_i^* \cdot \mathrm{Im}\ \mathbf{G}(\mathbf{r}_i, \mathbf{r}_j, \omega_p) \cdot \mathbf{d}_j$. Each atom can also decay into non-GMs, including free space, with a decay rate Γ'. The appearance of the real and imaginary parts of the Green's function in the coherent and dissipative terms has the classical analog that the in-phase and out of phase components of a field with respect to an oscillating dipole store time-averaged energy and perform time-averaged work, respectively. Because the first term in Eq. **1** is diagonal, the atomic coherences can be understood in terms of the eigenvalues $\{\lambda_\xi\}$ for $\xi = \{1, \cdots, N\}$ and the eigenfunctions of the matrix $\mathfrak{g}$, which has elements that are g_{ij}; the real and imaginary parts of $\{\lambda_\xi\}$ correspond to frequency shifts and GM decay rates, respectively, of the collective atomic mode ξ.

The transmission spectrum can be expressed in terms of the eigenvalues of $\mathfrak{g}$ as (39) (*SI Text*)

$$\frac{t(\tilde{\Delta}_A, N)}{t_0(\tilde{\Delta}_A)} = \prod_{\xi=1}^{N}\left(\frac{\tilde{\Delta}_A + \mathrm{i}\Gamma'/2}{\tilde{\Delta}_A + \mathrm{i}\Gamma'/2 + \lambda_\xi}\right), \qquad [2]$$

where $t_0(\tilde{\Delta}_A)$ is the transmission without atoms. In the case of a single atom i, the only eigenvalue is proportional to the self-Green's function, $\lambda_\xi = g_{ii}$, which implies that the transmission spectrum is a direct measurement of the self-Green's function at the atom's position. For noninteracting atoms, the off-diagonal elements of $\mathfrak{g}$ are zero, and thus, the eigenvalues are single-atom quantities, $\lambda_\xi = g_{ii}$, because there is no cooperative response.

In contrast, for interacting atoms, the off-diagonal elements are nonnegligible, and there is a cooperative response. In particular, for the atomic frequency inside the bandgap of a photonic crystal, the elements g_{ij} are well-approximated by (28)

$$g_{ij} = \left(J_{1D} + \frac{\mathrm{i}\Gamma_{1D}}{2}\right)\cos\left(\frac{\pi x_i}{a}\right)\cos\left(\frac{\pi x_j}{a}\right)e^{-\kappa_x |x_i - x_j|}, \qquad [3]$$

where the cosine factors arise from the Bloch mode, and the decay length $1/\kappa_x$ is caused by the exponential decay of the field and results in a finite range of interaction. For an infinite photonic crystal, $\Gamma_{1D} = 0$, because the light is localized, and there is no dissipation through the GM. However, for a finite PCW of length L, the GM dissipation $\Gamma_{1D} \sim e^{-\kappa_x L}$ is finite because of leakage of the mode out of the edges of the structure.

In the limit where the interaction range $1/\kappa_x$ is much larger than the separation $\delta x_{ij} = |x_i - x_j|$ of the atoms, $\kappa_x\ \delta x_{ij} \lesssim \kappa_x\ \Delta x_A \ll 1$, the GM input field couples predominantly to a single collective "bright" mode of the system with eigenvalue $\lambda_B = \sum_{i=1}^{N} g_{ii} = \sum_{i=1}^{N}(J^{ii}_{1D} + \mathrm{i}\,\Gamma^{ii}_{1D}/2)$. Formally, when $\kappa_x = 0$, the matrix $\mathfrak{g}$ is separable [$g_{ij} = u_i u_j$ with $u_i \propto \cos(\pi x_i/a)$] and therefore, only has one nonzero eigenvalue. In this single bright mode approximation, the transmission spectrum is given by

$$\frac{t(\tilde{\Delta}_A, N)}{t_0(\tilde{\Delta}_A)} = \frac{\tilde{\Delta}_A + \mathrm{i}\Gamma'/2}{\left(\tilde{\Delta}_A + \sum_{I=1}^{N} J^{ii}_{1D}\right) + \mathrm{i}\left(\Gamma' + \sum_{i=1}^{N}\Gamma^{ii}_{1D}\right)\Big/2}. \qquad [4]$$

We have confirmed numerically that this single bright mode picture is valid within the limits of our uncertainties for the range of frequencies of the measured spectra in Fig. 3. In particular, at the largest detuning into the bandgap $\Delta_{BE} = 60$ GHz, we have $\kappa_x\ \Delta x_A \simeq 0.2$. However, for atomic frequencies farther away from the band edge, this approximation eventually breaks down (e.g., at the bandgap center, $\kappa_x\ \Delta x_A \simeq 1.5$).

The single bright mode approximation is also valid in conventional CQED. The Green's function matrix is then given by $g_{ij} = (J_{1D} + \mathrm{i}\Gamma_{1D}/2)\ \cos(k_c x_i)\cos(k_c x_j)$, where k_c is the wavevector of the standing wave cavity. In this case, $J_{1D} \propto \Delta_c/(1 + \Delta_c^2/\gamma_c^2)$ and $\Gamma_{1D} \propto \gamma_c/(1 + \Delta_c^2/\gamma_c^2)$, where Δ_c is the detuning from the cavity resonance and γ_c is the cavity linewidth. Importantly, the ratio of the imaginary dissipative coupling rate to the real coherent coupling rate falls off with inverse detuning, $R_{CQED} = \Gamma_{1D}/J_{1D} = \gamma_c/\Delta_c$ for large Δ_c, whereas in a PCW bandgap, the fall off is exponential with detuning from the band edge.

Analysis of Measured Spectra

Eq. **4** provides a direct mapping between the observed transmission spectra in Fig. 3 *B–D* and the electromagnetic Green's function of the PCW. In particular, the line shape is Lorentzian for purely dissipative dynamics ($J^{ii}_{1D} = 0$). This line shape is precisely what occurs at the frequency of the first cavity mode ν_1, as shown in Fig. 3*B*. When the GM band edge frequency is moved toward the atomic resonance ν_{D1}, the dispersive interactions are switched on, and the transmission line shape becomes asymmetric, displaying

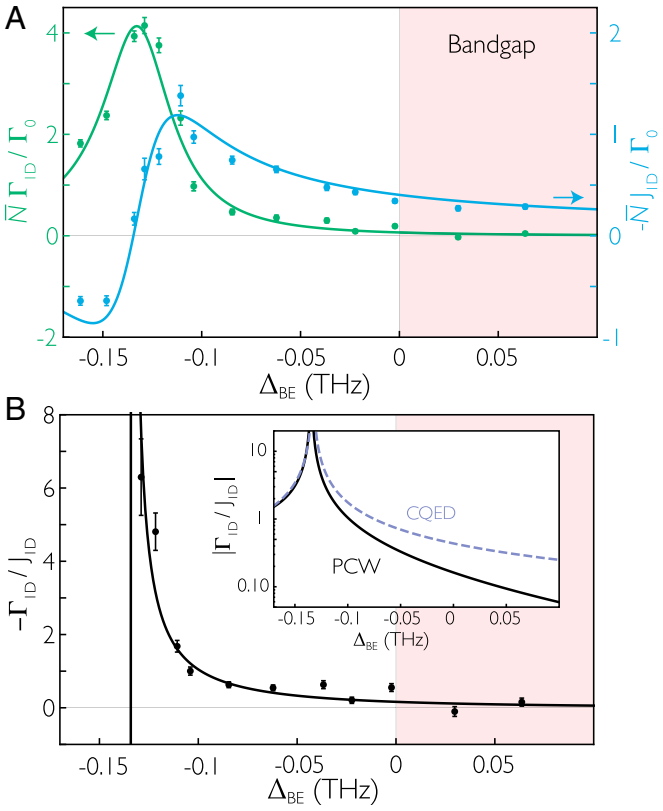

Fig. 4. (*A*) Peak dissipative interaction rate $\bar{N}\Gamma_{1D}$ (green) and coherent rate $\bar{N}J_{1D}$ (blue) around the band edge. With $\bar{N}$ determined from independent decay rate measurements, the values for Γ_{1D}, J_{1D} are found from fits of the transmission model in Eq. **4** to the measured atomic spectra and normalized by the free space decay rate $\Gamma_0 = 2\pi \times 4.56$ MHz for the Cs D_1 line. The lines are the predictions from a numerical model based on 1D transfer matrices. (*B*) The measured and calculated ratios $\mathcal{R} = \Gamma_{1D}/J_{1D}$. The average of the two points in the bandgap gives a ratio of the dissipative to coherent coupling rate $\mathcal{R} = 0.05 \pm 0.17$. *B*, *Inset* is a comparison of $\mathcal{R}$ for the PCW calculation (solid line) and CQED model (dashed line). From the measured linewidth of the first cavity resonance, $\gamma_c = 60 \pm 8$ GHz, CQED predicts that $\mathcal{R}_{CQED} = \gamma_c/\Delta_c$, where $\Delta_c = (\nu_p - \nu_1)$. Note that $-J_{1D}$ is plotted to more readily compare Γ_{1D} and J_{1D} as the band edge is approached.

a Fano-like resonance (46), which can be observed in Fig. 3 *C* and *D*. The appearance of an asymmetry in the atomic spectra directly reveals a significant coherent coupling rate J_{1D}, which is evident for frequencies that are in the bandgap region.

For all relevant frequencies, the spectra for the TM GM are approximately symmetric, since $J_{1D}^{TM} \ll \Gamma_{1D}^{TM} \ll \Gamma'$ for this GM polarization. An example of a TM spectrum is shown as the gray curve in Fig. 3*B*. Because the TM bandgap is so far detuned, the TM spectra are insensitive to Δ_{BE} and serve as a calibration signal. Using a waveguide transmission model, we fit the TM transmission spectra and extract a TM GM decay rate of $\Gamma_{1D}^{TM} = (0.045 \pm .01)\ \Gamma_0$. This rate is ~30 times smaller than the TE GM decay rate Γ_{1D} at the first resonance ν_1. The ratio $\Gamma_{1D}^{TE}/\Gamma_{1D}^{TM} \approx 30$ is explained well by the expected slow-light and cavity enhancement of the PCW described in ref. 21 and *SI Text*. From the TM fits, we also measure $\Gamma' = 2\pi \times 9.1$ MHz, which because of inhomogeneous broadening, is larger than the value $\Gamma' = 2\pi \times 5.0$ MHz predicted from FDTD numerical calculations (*SI Text*). While tuning the band edge to move the atomic frequency ν_{D1} into the bandgap, TM spectra are measured to confirm in situ that the average atom number is approximately constant over the course of the measurements of TE spectra.

To obtain quantitative values for the collective frequency shifts and decay rates by fitting the TE atomic spectra to the spin model, we must account for the fluctuations in atom number and position along the x axis. As depicted in Figs. 1*A* and 2*C*, trapped atoms are approximately free to move along the axis of the device (*SI Text*). Their coupling rates are thus modulated by the fast oscillation of the Bloch function, which near the band edge, is approximately given by Eq. **3**, $\Gamma_{1D}^{ii}(x_i) = \Gamma_{1D}\cos^2(x_i\pi/a)$, and $J_{1D}^{ii}(x_i) = J_{1D}\cos^2(x_i\pi/a)$. Here, Γ_{1D} and J_{1D} are the peak values. Furthermore, although we know the average atom number $\bar{N} = 3.0 \pm 0.5$ atoms from independent decay rate measurements (*SI Text*), the atom number for each experiment follows an unknown distribution. To model the experimental transmission spectra, such as in Fig. 3, we average the expression in Eq. **4** over the atom positions $\{x_i\}$ along the Bloch function and assume a Poisson distribution $P_{\bar{N}}(N)$ for the atom number N. We extract peak values Γ_{1D} and J_{1D} and plot the resulting cooperative rates $\bar{N}\Gamma_{1D}$ and $\bar{N}J_{1D}$ in Fig. 4*A*. In particular, at the first resonance ν_1, the fitted single-atom GM decay rate is $\Gamma_{1D} = (1.4 \pm 0.2)\ \Gamma_0$, which is in good agreement with the decay time measurements $\Gamma_{1D} = (1.5 \pm 0.2)\ \Gamma_0$. More generally, we find good agreement between our measurements and our model for the transmission, as shown in Fig. 3.

The ratio $\mathcal{R} = \Gamma_{1D}/J_{1D}$ is shown in Fig. 4*B*. Because of the evanescent nature of the field in the bandgap, $\mathcal{R}$ decays exponentially with increasing detuning into the bandgap, $\mathcal{R} \sim e^{-\kappa_x L}$, where $\kappa_x \propto \sqrt{\Delta_{BE}}$ (28). As displayed in Fig. 4*B*, *Inset*, the ratio between the GM decay rate Γ_{1D} to the GM frequency shift J_{1D} diminishes much faster than would be the case in traditional settings, such as CQED, for which $\mathcal{R}_{CQED} = \gamma_c/\Delta_c$, where γ_c is the cavity linewidth and Δ_c is the detuning from the cavity resonance. Indeed, by performing an average of the last two measured frequencies in the bandgap, we obtain $\mathcal{R} = 0.05 \pm 0.17$, whereas $\mathcal{R}_{CQED} = 0.30 \pm 0.04$, where we have taken the cavity linewidth to be a value consistent with the linewidth of the first cavity mode of the PCW ($\gamma_c = 60 \pm 8$ GHz). We can then infer that the ratio of dispersive to dissipative rates for GM atom–atom interactions (i.e., $1/\mathcal{R}$) is significantly larger than is the case in conventional optical physics (e.g., CQED).

Beyond the detailed modeling involving Eq. **4** averaged over fluctuations in atom number and position, we also fit the spectra with a generic transmission model with no averaging, as shown in *SI Text*. We find that the effective values for the GM decay rate and frequency shift are related to $\bar{N}\Gamma_{1D}$ and $\bar{N}J_{1D}$ in Fig. 4*A* by a simple scale factor related to the averaging of the Bloch function $\cos^2(\pi x/a)$.

Despite favorable scaling between the collective frequency shifts and the GM decay rates, there is still one obstacle to overcome toward purely dispersive atomic interactions, namely atomic emission into non-GMs (characterized by Γ'). For this PCW structure, the FDTD-simulated value of this decay rate is $\Gamma' \simeq 1.1\ \Gamma_0$ (21) for the relevant frequencies of our experiment. Fortunately, it has been shown that suitable engineering of a wide variety of nanophotonic structures can lead to significant reductions in Γ'/Γ_0 (47). For example, ref. 1 reviews possibilities to achieve $\Gamma' \simeq 0.1\Gamma_0$.

Concluding Remarks and Outlook

In conclusion, we report the initial observation of cooperative atom interactions in the bandgap of a PCW. By tuning the band edge frequency of the PCW, we are able to modify the interactions between the atoms that are trapped close to the device, reducing the dissipative relative to coherent coupling for frequencies inside the bandgap of the PCW. Equipped with a theoretical model based on the electromagnetic Green's function of the alligator PCW, we infer quantitative values for the collective frequency shifts and decay rates experienced by the atoms. Moreover, we infer a suppression of the dissipative interactions with respect to the coherent ones several times larger than is customarily obtained in atomic physics. This measurement provides the first stepping stone toward the realization of quantum many-body physics in bandgap systems.

Moreover, near-term extensions of our experiment open the door to exploring new physical scenarios by using atoms coupled to PCWs. By trapping the atoms at the center of the device with GMs (47), we expect a sixfold increase to both coupling strengths J_{1D} and Γ_{1D} relative to Γ'. Moreover, by probing the atoms with the Cs D_2 line tuned to the upper band edge, where the intensity at the position of the atoms is larger, we expect a further improvement by a factor of two. Combining these two effects, we expect a significant enhancement of interactions through GMs compared with conventional free space interactions, namely $J_{1D}, \Gamma_{1D} > 10 \times \Gamma'$. This improvement could enable investigations of new paradigms for atom–photon interactions (28, 29, 36), including the recently proposed multiphoton dressed states (26, 27).

Note. After the submission of this manuscript, ref. 48 reported measurements of transmission spectra for a superconducting qubit placed within the bandgap of a microwave photonic crystal.

ACKNOWLEDGMENTS. We acknowledge the contributions of O. J. Painter and his group, including for fabrication and clean room facilities. We also acknowledge A. Burgers, C.-L. Hung, J. Laurat, M. J. Martin, A. C. McClung, J. A. Muniz, and L. Peng. Funding was provided by National Science Foundation (NSF) Grant PHY 1205729; by the Air Force Office of Scientific Research Multidisciplinary University Research Initiative (MURI) for Quantum Memories in Photon-Atomic Solid-State Systems (QuMPASS); by the Institute for Quantum Information and Matter (IQIM), NSF Physics Frontiers Center with support of the Moore Foundation; by the Office of Naval Research (ONR) Award N00014-16-1-2399; by the ONR MURI for Quantum Opto-Mechanics with Atoms and Nanostructured Diamond (QOMAND); and by the Department of Defense National Security Science and Engineering Faculty Fellowship (NSSEFF) Program. A.G. was supported by the Nakajima Foundation. A.A.-G. and M.L. were supported by the IQIM Postdoctoral Fellowship. A.A.-G. also acknowledges support from Global Marie Curie Fellowship LANTERN 655701. S.-P.Y. acknowledges support from the International Fulbright Science and Technology Award. D.E.C. acknowledges support from Fundacio Privada Cellex Barcelona, Marie Curie CIG ATOMNANO, MINECO Severo Ochoa Grant SEV-2015-0522, and ERC Starting Grant FoQAL.

1. Lodahl P, Mahmoodian S, Stobbe S (2015) Interfacing single photons and single quantum dots with photonic nanostructures. *Rev Mod Phys* 87(2):347.
2. Kimble HJ (2008) The quantum internet. *Nature* 453(7198):1023–1030.
3. Vuckovic J, Yamamoto Y (2003) Photonic crystal microcavities for cavity quantum electrodynamics with a single quantum dot. *Appl Phys Lett* 82(15):2374–2376.
4. Yoshie T, et al. (2004) Vacuum Rabi splitting with a single quantum dot in a photonic crystal nanocavity. *Nature* 432(7014):200–203.
5. Aoki T, et al. (2006) Observation of strong coupling between one atom and a monolithic microresonator. *Nature* 443(7112):671–674.
6. Hennessy K, et al. (2007) Quantum nature of a strongly coupled single quantum dot-cavity system. *Nature* 445(7130):896–899.
7. Thompson JD, et al. (2013) Coupling a single trapped atom to a nanoscale optical cavity. *Science* 340(6137):1202–1205.
8. Bajcsy M, et al. (2009) Efficient all-optical switching using slow light within a hollow fiber. *Phys Rev Lett* 102(20):203902.
9. Balykin VI, Hakuta K, Kien FL, Liang JQ, Morinaga M (2004) Atom trapping and guiding with a subwavelength-diameter optical fiber. *Phys Rev A* 70(1):011401.
10. Londero P, Venkataraman V, Bhagwat AR, Slepkov AD, Gaeta AL (2009) Ultralow-power four-wave mixing with Rb in a hollow-core photonic band-gap fiber. *Phys Rev Lett* 103(4):043602.
11. Vetsch E, et al. (2010) Optical interface created by laser-cooled atoms trapped in the evanescent field surrounding an optical nanofiber. *Phys Rev Lett* 104(20):203603.
12. Goban A, et al. (2012) Demonstration of a state-insensitive, compensated nanofiber trap. *Phys Rev Lett* 109(3):033603.
13. Sørensen HL, et al. (2016) Coherent backscattering of light off one-dimensional atomic strings. arXiv:1601.04869.
14. Chang DE, Sørensen AS, Demler EA, Lukin MD (2007) A single-photon transistor using nanoscale surface plasmons. *Nat Phys* 3(11):807–812.
15. Akimov AV, et al. (2007) Generation of single optical plasmons in metallic nanowires coupled to quantum dots. *Nature* 450(7168):402–406.
16. Huck A, Kumar S, Shakoor A, Andersen UL (2011) Controlled coupling of a single nitrogen-vacancy center to a silver nanowire. *Phys Rev Lett* 106(9):096801.
17. Wallraff A, et al. (2004) Strong coupling of a single photon to a superconducting qubit using circuit quantum electrodynamics. *Nature* 431(7005):162–167.
18. van Loo AF, et al. (2013) Photon-mediated interactions between distant artificial atoms. *Science* 342(6165):1494–1496.
19. Devoret MH, Schoelkopf RJ (2013) Superconducting circuits for quantum information: An outlook. *Science* 339(6124):1169–1174.
20. Joannopoulos JD, Meade RD, Winn JN (1995) *Photonic Crystals: Molding the Flow of Light* (Princeton Univ Press, Singapore).
21. Goban A, et al. (2015) Superradiance for atoms trapped along a photonic crystal waveguide. *Phys Rev Lett* 115(6):063601.
22. Yablonovitch E (1987) Inhibited spontaneous emission in solid-state physics and electronics. *Phys Rev Lett* 58(20):2059–2062.
23. John S (1987) Strong localization of photons in certain disordered dielectric superlattices. *Phys Rev Lett* 58(23):2486–2489.
24. John S, Wang J (1990) Quantum electrodynamics near a photonic band gap: Photon bound states and dressed atoms. *Phys Rev Lett* 64(20):2418–2421.
25. Kurizki G (1990) Two-atom resonant radiative coupling in photonic band structures. *Phys Rev A* 42(5):2915–2924.
26. Shi T, Wu YH, Gonzalez-Tudela A, Cirac JI (2016) Bound states in boson impurity models. *Phys Rev X* 6(2):021027.
27. Calajó G, Ciccarello F, Chang DE, Rabl P (2016) Atom-field dressed states in slow-light waveguide QED. *Phys Rev A* 93(3):033833.
28. Douglas JS, et al. (2015) Quantum many-body models with cold atoms coupled to photonic crystals. *Nat Photonics* 9(5):326–331.
29. González-Tudela A, Hung CL, Chang DE, Cirac JI, Kimble HJ (2015) Subwavelength vacuum lattices and atom-atom interactions in two-dimensional photonic crystals. *Nat Photonics* 9(5):320–325.
30. Hartmann MJ, Brandao FGSL, Plenio MB (2006) Strongly interacting polaritons in coupled arrays of cavities. *Nat Phys* 2(12):849–855.
31. Greentree AD, Tahan C, Cole JH, Hollenberg LCL (2006) Quantum phase transitions of light. *Nat Commun* 2(12):856–861.
32. Goban A, et al. (2014) Atom-light interactions in photonic crystals. *Nat Commun* 5:3808.
33. Yu SP, et al. (2014) Nanowire photonic crystal waveguides for single-atom trapping and strong light-matter interactions. *Appl Phys Lett* 104(11):111103.
34. Lund-Hansen T, et al. (2008) Experimental realization of highly efficient broadband coupling of single quantum dots to a photonic crystal waveguide. *Phys Rev Lett* 101(11):113903.
35. Young AB, et al. (2015) Polarization engineering in photonic crystal waveguides for spin-photon entanglers. *Phys Rev Lett* 115(15):153901.
36. Hung CL, González-Tudela A, Cirac JI, Kimble HJ (2016) Quantum spin dynamics with pairwise-tunable, long-range interactions. *Proc Natl Acad Sci USA* 113(34):E4946–E4955.
37. Lumerical Solutions, Inc. (2015) Version 8.12. http://www.lumerical.com/tcad-products/fdtd/.
38. COMSOL Inc. (2009) COMSOL Multiphysics (COMSOL AB, Stockholm), Version 3.5a.
39. Asenjo-Garcia A, Hood JD, Chang DE, Kimble HJ (2016) Atom-light interactions in quasi-1D dielectrics: A Green's function perspective. arXiv:1606.04977.
40. Shen JT, Fan S (2005) Coherent photon transport from spontaneous emission in one-dimensional waveguides. *Opt Lett* 30(15):2001–2003.
41. Gardiner CW, Collett MJ (1985) Input and output in damped quantum systems: Quantum stochastic differential equations and the master equation. *Phys Rev A Gen Phys* 31(6):3761–3774.
42. Dung HT, Knöll L, Welsch DG (2002) Resonant dipole-dipole interaction in the presence of dispersing and absorbing surroundings. *Phys Rev A* 66(6):063810.
43. Buhmann SY, Welsch DG (2007) Dispersion forces in macroscopic quantum electrodynamics. *Prog Quantum Electron* 31(2):51–130.
44. Dzsotjan D, Sørensen AS, Fleischhauer M (2010) Quantum emitters coupled to surface plasmons of a nanowire: A Green's function approach. *Phys Rev B* 82(7):075427.
45. Novotny L, Hecht B (2006) *Principles of Nano-Optics* (Cambridge Univ Press, New York).
46. Fano U (1961) Effects of configuration interaction on intensities and phase shifts. *Phys Rev* 124(6):1866–1878.
47. Hung C-L, Meenehan SM, Chang DE, Painter O, Kimble HJ (2013) Trapped atoms in one-dimensional photonic crystals. *New J Phys* 15(8):083026.
48. Liu Y, Houck AA (August 1, 2016) Quantum electrodynamics near a photonic band-gap. *Nat Phys*, 10.1038/nphys3834.
49. Tuchendler C, Lance AM, Browaeys A, Sortais YRP, Grangier P (2008) Energy distribution and cooling of a single atom in an optical tweezer. *Phys Rev A* 78(3):033425.